AGU PUBLICATIONS

Geophysical Research Letters

RESEARCH LETTER
10.1002/2017GL074897

Key Points:
- Simultaneous MEX and MAVEN observations demonstrate that the Martian ionosphere responds quickly to an interplanetary shock passage
- The response time is consistent with propagation of a pressure pulse from the bow shock to the ionosphere in the fast magnetosonic mode
- Remote soundings reveal the presence of irregular structures in the topside ionosphere shortly after the shock passage

Correspondence to:
Y. Harada,
yuki-harada@uiowa.edu

Citation:
Harada, Y., et al. (2017), Dynamic response of the Martian ionosphere to an interplanetary shock: Mars Express and MAVEN observations, *Geophys. Res. Lett.*, *44*, 9116–9123, doi:10.1002/2017GL074897.

Received 10 JUL 2017
Accepted 23 AUG 2017
Accepted article online 29 AUG 2017
Published online 18 SEP 2017

Dynamic response of the Martian ionosphere to an interplanetary shock: Mars Express and MAVEN observations

Y. Harada[1], D. A. Gurnett[1], A. J. Kopf[1], J. S. Halekas[1], S. Ruhunusiri[1], C. O. Lee[2], T. Hara[2], J. Espley[3], G. A. DiBraccio[3], D. L. Mitchell[2], C. Mazelle[4], D. E. Larson[2], and B. M. Jakosky[5]

[1]Department of Physics and Astronomy, University of Iowa, Iowa City, Iowa, USA, [2]Space Sciences Laboratory, University of California, Berkeley, California, USA, [3]NASA Goddard Space Flight Center, Greenbelt, Maryland, USA, [4]IRAP, University of Toulouse, CNRS, UPS, CNES, Toulouse, France, [5]Laboratory for Atmospheric and Space Physics, University of Colorado Boulder, Boulder, Colorado, USA

Abstract Multipoint observations from the Mars Advanced Radar for Subsurface and Ionosphere Sounding (MARSIS) instrument on board Mars Express and the Mars Atmosphere and Volatile EvolutioN (MAVEN) mission reveal a dynamic response of the Martian ionosphere to abrupt variations in the upstream solar wind plasma. On 2 February 2017, MAVEN, located upstream from the Martian bow shock, encountered a corotating interaction region-related interplanetary shock with a sudden enhancement in the dynamic pressure. MARSIS, operating in the upper ionosphere at ~478 km altitudes and ~78° solar zenith angles, observed a sharp increase in the local magnetic field magnitude ~1 min after the shock passage at MAVEN. The time lag is roughly consistent with the expected propagation time of a pressure pulse from the bow shock to the upper ionosphere at the fast magnetosonic speed. Subsequently, remote soundings recorded disturbed signatures of the topside ionosphere below Mars Express.

1. Introduction

The solar wind interaction with the upper atmosphere of Mars forms a dynamic system in which the structure of the ionosphere and magnetosphere can vary significantly in response to time-varying solar wind and interplanetary magnetic field (IMF) conditions. A number of studies have been dedicated to investigate the response of the Mars-solar wind system to space weather events such as corotating interaction regions (CIRs) [*Dubinin et al.*, 2009; *Edberg et al.*, 2010; *Hara et al.*, 2011; *Opgenoorth et al.*, 2013; *Diéval et al.*, 2013], interplanetary coronal mass ejections [*Morgan et al.*, 2014; *Jakosky et al.*, 2015a; *Curry et al.*, 2015; *Sánchez-Cano et al.*, 2017], and solar energetic particle events [*Espley et al.*, 2007; *Futaana et al.*, 2008; *Ulusen et al.*, 2012; *Němec et al.*, 2014; *Schneider et al.*, 2015]. The observed responses include perturbations in the ionosphere and magnetosphere, compression of boundaries, reduction (enhancement) in the precipitation of solar wind (heavy) ions due to finite gyroradius effects, increases in the ionization rates and energy deposition at low altitudes, and enhancements of piled up magnetic fields and planetary ion escape.

One of the key issues concerning the dynamics of the Mars plasma environment during space weather events involves the response time scale of the Martian ionosphere and magnetosphere to the upstream solar wind and IMF variations. However, observational investigation on this issue with single-point, in situ measurements has been limited primarily by spacecraft orbital periods (typically several hours), which are much longer than the expected response time scale of the order of minutes [e.g., *Modolo et al.*, 2012; *Ma et al.*, 2014]. From remote measurements using energetic neutral atoms along with simultaneous solar wind electron monitoring, *Futaana et al.* [2006] showed that the induced magnetosphere boundary was compressed almost instantaneously as an interplanetary shock arrived at Mars. At Venus, multipoint magnetic field measurements were utilized to determine the time scale of ~10 min for the nightside magnetotail to reconfigure in response to variations in the IMF directions [*Huddleston et al.*, 1996; *Slavin et al.*, 2009].

In this paper, we investigate the response of the dayside upper ionosphere of Mars to an interplanetary shock passage on 2 February 2017 with a particular emphasis on determining the response time scale. We analyze 7.54 s cadence ionospheric sounding data from the Mars Advanced Radar for Subsurface and Ionosphere

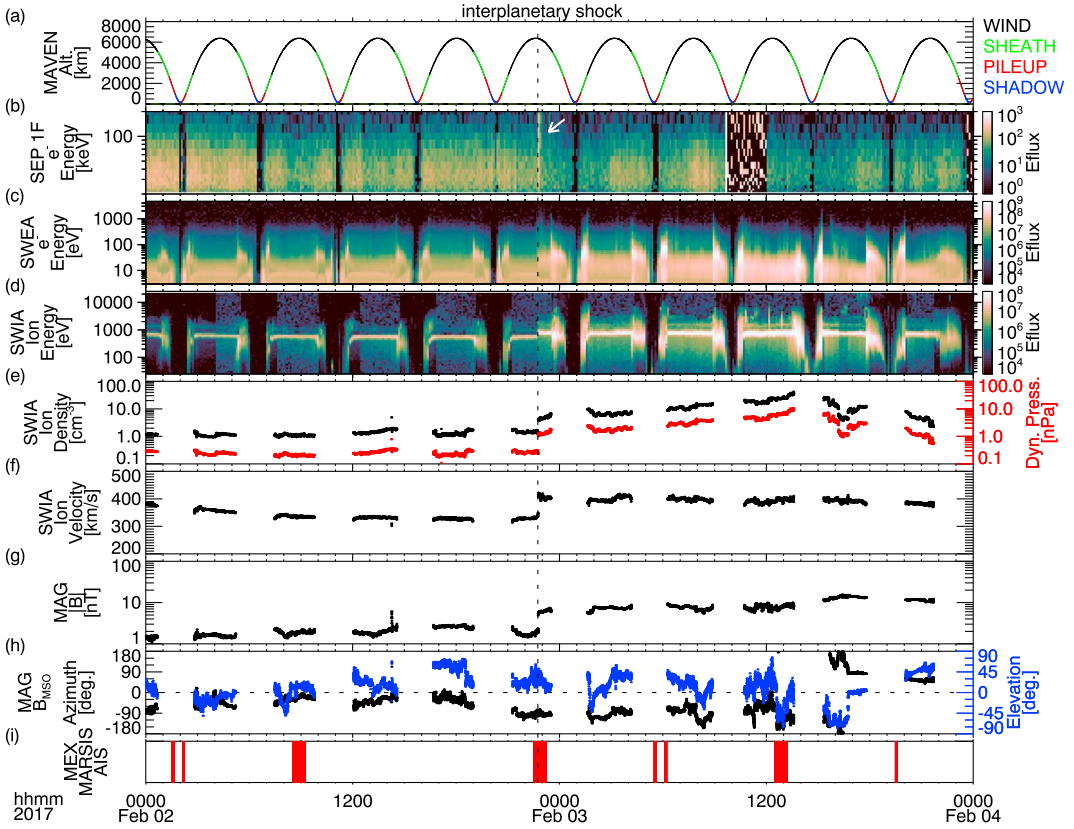

Figure 1. MAVEN observations of the upstream solar wind and IMF on 2–3 February 2017. Time series of (a) MAVEN altitudes with different colors denoting different plasma regions based on the nominal positions of the bow shock and magnetic pileup boundary [*Trotignon et al.*, 2006], energy spectra in units of differential energy flux (Eflux) of eV/cm^2/s/sr/eV of (b) high-energy electrons from the SEP 1-Forward (1F) field of view, (c) low-energy, omnidirectional electrons from SWEA, and (d) omnidirectional ions from SWIA, solar wind measurements of (e) ion density and dynamic pressure, (f) ion velocity, (g) magnetic field magnitude, and (h) magnetic field directions. Note that the SEP 1 attenuator was closed during ~10–12 UT on 3 February. The red bars in Figure 1i show the time segments during which MARSIS operated in the AIS mode. The vertical dashed line marks the arrival of an interplanetary shock at MAVEN.

Sounding (MARSIS) instrument on board Mars Express [*Gurnett et al.*, 2008; *Jordan et al.*, 2009; *Orosei et al.*, 2015] in combination with upstream plasma and field measurements by the Mars Atmosphere and Volatile EvolutioN (MAVEN) mission [*Jakosky et al.*, 2015b], including 32 Hz magnetic field data obtained by the magnetometer (MAG) [*Connerney et al.*, 2015] and 2–4 s resolution upstream particle measurements by the solar wind ion analyzer (SWIA) [*Halekas et al.*, 2015], solar wind electron analyzer (SWEA) [*Mitchell et al.*, 2016], and solar energetic particle (SEP) [*Larson et al.*, 2015] instruments. In the MARSIS Active Ionospheric Sounder (AIS) mode, the radar conducts ionospheric sounding by transmitting a short electromagnetic pulse at a fixed frequency and then measuring a wave reflected from the topside ionosphere. The sounding frequency is stepped over 160 frequencies between 0.1 and 5.5 MHz in 1.26 s, and this cycle is repeated every 7.54 s. SWIA measures ions with energies from 25 eV to 25 keV, SWEA measures electrons with energies from 3 eV to 4.6 keV, and SEP measures 20–6000 keV ions and 20–1000 keV electrons. These multipoint, high time resolution measurements enable comprehensive characterization of both the driving interplanetary shock and the dynamic response of the Martian ionosphere.

2. Observations

2.1. Passage of An Interplanetary Shock on 2 February 2017

Figure 1 presents an overview of the solar wind and IMF conditions during 2–3 February 2017 from MAVEN observations. In Figures 1e–1h, we show ion and IMF parameters for solar wind intervals of the MAVEN orbits, selected visually, based on the electron and ion energy spectrograms (Figures 1c and 1d). We observed abrupt jumps in solar wind density (Figure 1e), velocity (Figure 1f), and IMF magnitude (Figure 1g) at 22:44:36 UT on

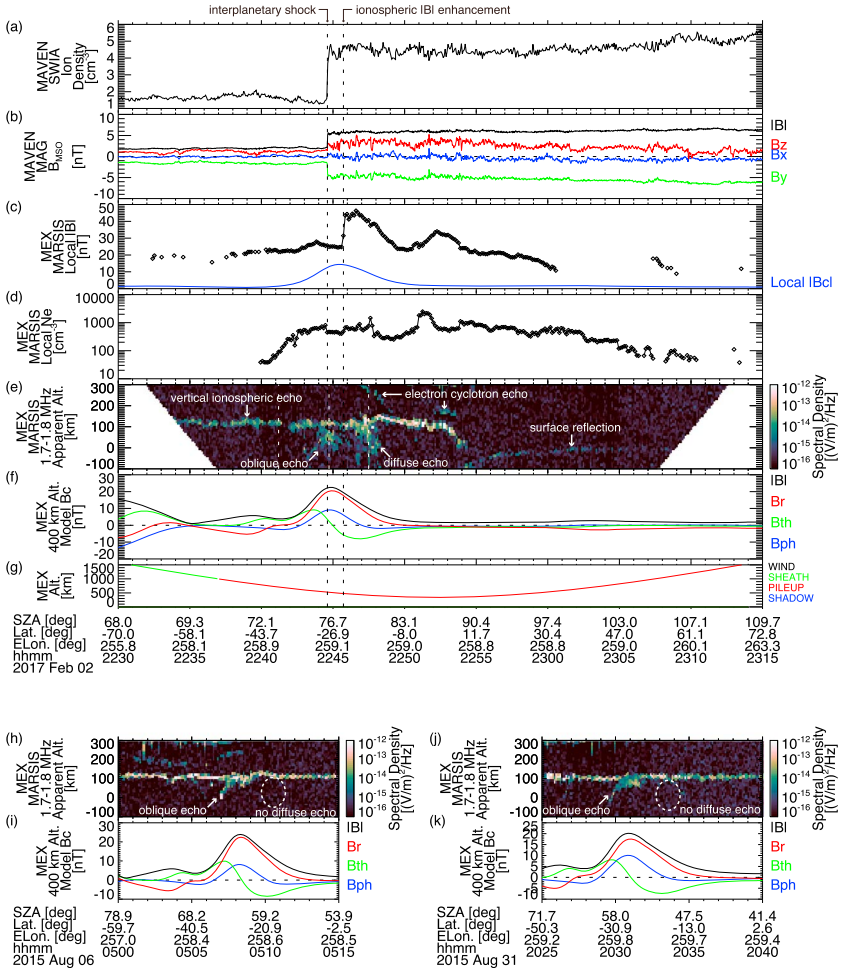

Figure 2. MAVEN observations of (a) solar wind density and (b) interplanetary magnetic field, and MARSIS observations of (c) local magnetic field magnitude, (d) local electron density, and (e) radargram (echo intensities as a function of apparent altitude and time) showing 1.7–1.8 MHz echoes, (f) crustal magnetic fields below Mars Express at a 400 km altitude computed from the spherical harmonic model by *Morschhauser et al.* [2014] (magnitude $|B|$ and spherical coordinate components B_r, B_θ, and B_ϕ, are shown as black, red, green, and blue lines, respectively), and (g) Mars Express altitude color coded in the same manner as Figure 1a. The Mars Express solar zenith angle, latitude, and east longitude are indicated in the text label. The blue line in Figure 2c shows the crustal field strength at the Mars Express altitude. The vertical dashed lines mark the interplanetary shock arrival at MAVEN at 22:44:36 UT and the local magnetic field enhancement at Mars Express at 22:45:43 UT. The white dashed lines in Figure 2e indicate the times at which the ionograms in Figure 4 were obtained. Radargrams and model crustal fields from other orbits above the same geographic location are shown in Figures 2h–2k.

2 February 2017 (indicated by the vertical dashed line in Figure 1), while the IMF direction remains almost unchanged (Figure 1h). This solar wind discontinuity is characterized by a factor of ~3 enhancement in the density and magnetic field and a factor of ~5 enhancement in the dynamic pressure (Figure 1e); the solar wind density changed from 1.4 cm^{-3} to 4.7 cm^{-3} with a solar wind speed increase from 342 km/s to 411 km/s, and the IMF magnitude increased from 2.0 nT to 5.8 nT. Additionally, a brief enhancement in the high-energy (~100 keV) electron flux was recorded at the discontinuity (seen as a vertical "spike" indicated by the white arrow Figure 1b). These observations indicate that an interplanetary shock swept past MAVEN. This interplanetary shock is mostly likely associated with a CIR, given the repetitive nature of large-scale structure with periodicity corresponding to the solar rotation (not shown). Fortunately, MARSIS operated in the AIS mode at the interplanetary shock passage (Figure 1i), providing local and remote measurements of the topside ionosphere.

Figures 2a and 2b show a zoom-in of the interplanetary shock passage. The orbital configuration of MAVEN and Mars Express in Mars Solar Orbital (MSO) coordinates during this time interval is shown in Figures 3a–3d.

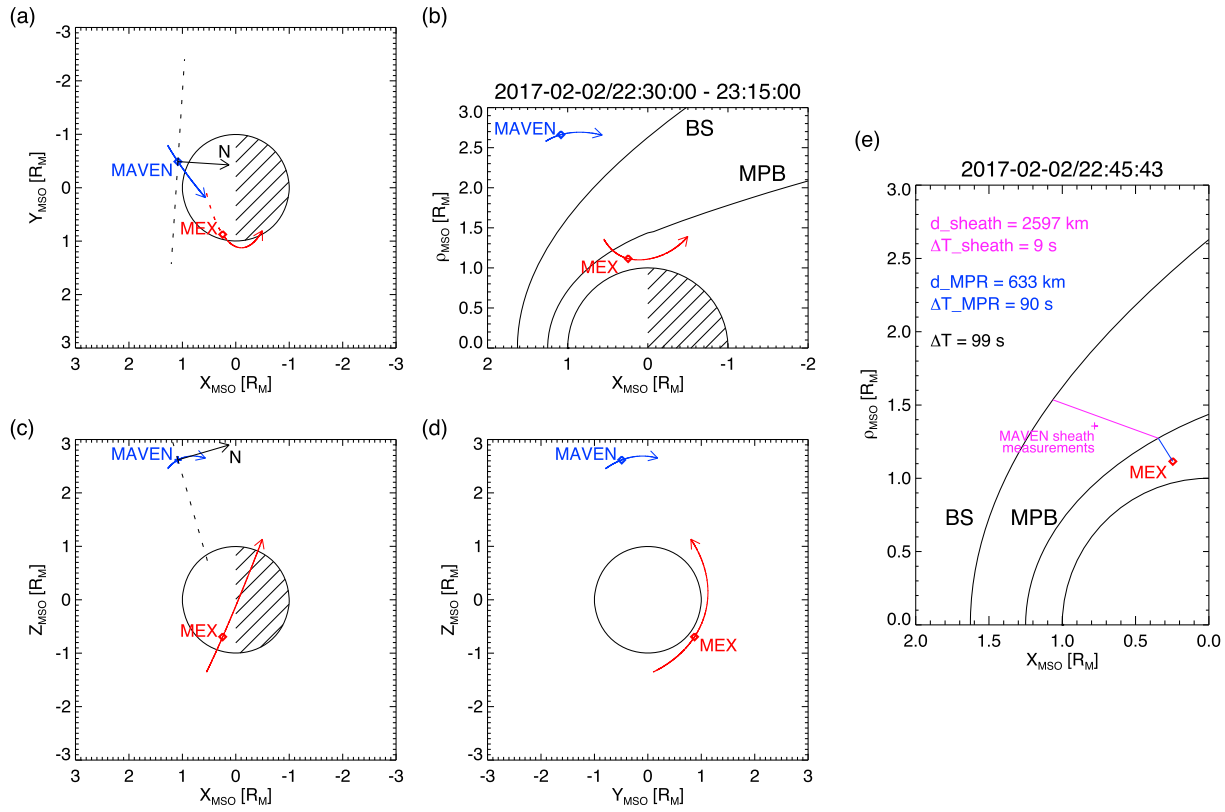

Figure 3. Orbital geometry of MAVEN and Mars Express in MSO coordinates during the time interval shown in Figure 2. The blue and red diamonds indicate the MAVEN location at 22:44:36 UT and the Mars Express location at 22:45:43 UT, respectively. The black arrows in Figures 3a and 3c show the interplanetary shock normal direction estimated from the minimum variance analysis of MAG data, and the dashed lines indicate its perpendicular lines, representing the intersections of the shock plane with the X_{MSO}-Y_{MSO} and X_{MSO}-Z_{MSO} planes including MAVEN. Figure 3e demonstrates a simple model calculation of the propagation time of a compressional pressure pulse traveling from the bow shock to Mars Express at the fast magnetosonic speed (see text for detail). The nominal positions of the bow shock and magnetic pileup boundary [*Trotignon et al.*, 2006] are shown in Figures 3b and 3e.

In the MSO coordinate system, the X axis points from Mars toward the Sun, Y points opposite to the direction of Mars' orbital velocity component perpendicular to X, and Z completes the orthogonal coordinate set. MAVEN was located near the apoapsis upstream from the bow shock, while Mars Express traveled from the magnetosheath into the upper ionosphere near the dusk terminator (Figures 3a–3d). The abrupt jumps in the solar wind density and IMF are seen at 22:44:36 UT as indicated by the first vertical dashed line in Figures 2a and 2b. The transition from one side to the other is very sharp, within less than 1 s based on 32 Hz MAG data (not shown). The minimum variance analysis [*Sonnerup and Cahill*, 1967] of the 32 Hz magnetic field data during 22:44:36–22:44:38 UT provides the shock normal (the minimum variance direction) $\mathbf{N} = [-0.958, 0.062, 0.282]$ MSO with an intermediate-to-minimum eigenvalue ratio of 10.5, indicating that the normal direction is well defined for this shock event. The shock normal direction is depicted by the black arrows in Figures 3a and 3c. The X_{MSO}-dominant shock normal direction is consistent with typical characteristics of CIR-related interplanetary shocks [*Berdichevsky et al.*, 2000]. If we assume that the interplanetary shock surface is planar and that it convects at the solar wind velocity, $\mathbf{V}_{SW}$, without any distortion by the presence of Mars, the convection time of the shock plane from the MAVEN location, $\mathbf{r}_{MAVEN}$, to Mars Express, $\mathbf{r}_{MEX}$, can be estimated as follows: $(\mathbf{r}_{MEX} - \mathbf{r}_{MAVEN}) \cdot \mathbf{N}/(\mathbf{V}_{SW} \cdot \mathbf{N}) \sim -0.4$ s. In other words, the shock geometry predicts almost the same arrival time at MAVEN and Mars Express under the "no Mars" assumption.

2.2. Response of the Martian Ionosphere to the Interplanetary Shock

Here we examine magnetic field and plasma parameters in the upper ionosphere from local measurements by MARSIS. Figure 2c shows the local magnetic field magnitude derived by the well-established method using so-called "electron cyclotron echoes" [*Gurnett et al.*, 2005, 2008, 2010; *Akalin et al.*, 2010]. At 22:45:43 UT indicated by the second vertical dashed line, when Mars Express was located at an altitude of ~478 km at a solar zenith angle of ~78°, MARSIS detected a sudden increase in the local magnetic field magnitude by a factor of

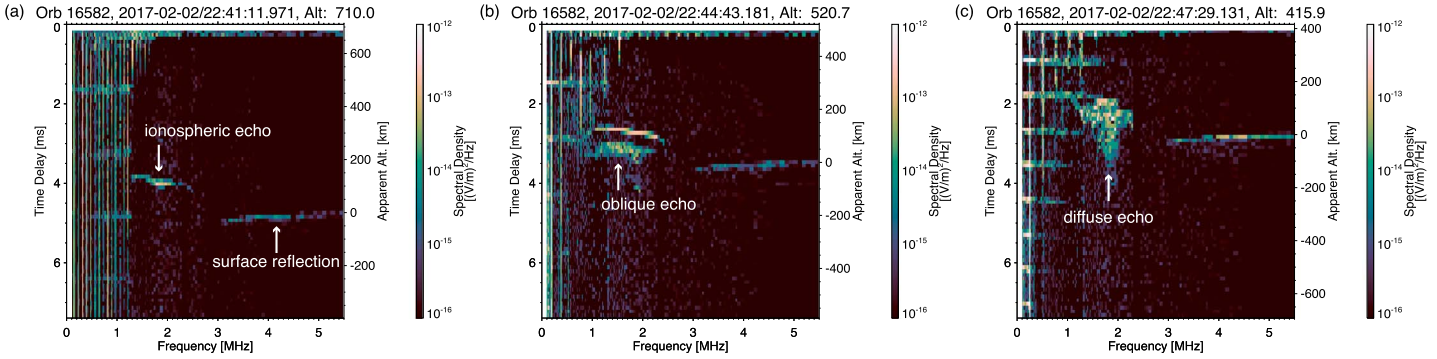

Figure 4. Ionograms (echo intensities as a function of time delay and frequency) obtained at (a) 22:41:11 UT, (b) 22:44:43 UT, and (c) 22:47:29 UT, which are indicated by the white dashed lines in Figure 2e.

1.8 from 25 nT to 44 nT within two 7.54 s steps. This magnetic field enhancement cannot be explained by a variation in local crustal field strengths (which reach only up to 14 nT at this location) as shown by the blue line in Figure 2c. Also, such a sharp, large variation is very rare in the MARSIS local magnetic field magnitude data. To examine how rare this event is, we performed a systematic search for similar sudden magnetic field jumps based on the following criteria: (i) $B_{1,min}/B_{2,max} > 1.5$ and $B_{1,min} - B_{2,max} > 15$ nT (corresponding to a field magnitude decrease with increasing time) or (ii) $B_{2,min}/B_{1,max} > 1.5$ and $B_{2,min} - B_{1,max} > 15$ nT (a field magnitude increase with increasing time), where $B_{1,min}$, $B_{1,max}$, $B_{2,min}$, and $B_{2,max}$ are the minimum (with subscript "min") and maximum ("max") magnetic field magnitudes in 1 min windows before ("1") a time step n and after ("2") the time step $n + 2$. This searching algorithm is optimized for sharp, step function-like variations by rejecting turbulent fluctuations [e.g., *Gurnett et al.*, 2010]. By applying this algorithm to over 10 years of the MARSIS derived data set, we found only one other noncrustal field jump event (7:16 UT on 3 January 2014) satisfying the criteria, demonstrating that such abrupt magnetic field jumps are uncommon. Meanwhile, at the same time as the sudden magnetic field enhancement, we find a factor of 1.6 increase from 409 cm^{-3} to 670 cm^{-3} in the local electron density data (Figure 2d) derived from plasma oscillation harmonics [*Gurnett et al.*, 2005, 2008, 2010; *Duru et al.*, 2008, 2011], but this variation is not particularly prominent compared to other density fluctuations during this orbit. To summarize the remarkable features of the MARSIS local measurements in the upper ionosphere, we observe the unusually abrupt and strong enhancement in the local magnetic field magnitude starting at some time between 22:45:35 and 22:45:43 UT, 59–67 s after the interplanetary shock passage at MAVEN.

Next we present remote measurements of the topside ionosphere from MARSIS. Figure 2e shows the echo intensity as a function of apparent altitude (the Mars Express altitude minus the apparent echo range uncorrected for dispersion) and time in a constant frequency range of 1.7–1.8 MHz (this format is called a radargram). This frequency range corresponds to electron densities of $3.6–4.0 \times 10^4$ cm^{-3}, probing the topside ionosphere typically at ~170–200 km altitudes on the dayside [e.g., *Morgan et al.*, 2008; *Ergun et al.*, 2015]. The relatively strong, narrow horizontal line at apparent altitudes of ~130 km in Figure 2e represents the ionospheric echo reflected vertically from a horizontally stratified ionosphere, while the weak, nearly horizontal line at ~0 km is the reflection from the Martian surface. Both signatures can be seen in Figure 4a, which shows an ionogram (displaying the echo intensity as a function of time delay and frequency) obtained at 22:41:11 UT well before the shock arrival at MAVEN. These are typical features of nominal topside sounding data. During 22:43:27–22:45:43 UT in Figure 2e, a secondary echo is seen below the main ionospheric echo with the highest apparent altitude located above the radially outward crustal magnetic field (Figure 2f). In the corresponding ionogram (Figure 4b), the secondary echo has a similar shape to the main ionospheric echo. These characteristics are very similar to those of the "oblique echoes" commonly observed above radial crustal magnetic field regions [*Gurnett et al.*, 2005; *Duru et al.*, 2006; *Nielsen et al.*, 2007; *Andrews et al.*, 2014; *Diéval et al.*, 2015; *Venkateswara Rao et al.*, 2017]. The oblique echoes were observed for other orbits traveling above the same location as demonstrated in Figures 2h–2k. Finally, shortly after the sudden enhancement in the local magnetic field magnitude, the width of the main ionospheric echo is considerably broadened at 22:46:36–22:48:14 UT (Figure 2e). The very diffuse nature of this ionospheric echo can be confirmed in the ionogram (Figure 4c). These "diffuse echoes" are interpreted as ionospheric echoes scattered with a broad range of incidence angles from highly irregular structures in the ionosphere [*Gurnett et al.*, 2008]. In contrast to

the oblique echoes, the diffuse echoes were absent at the same location for the orbits shown in Figures 2h–2k, suggesting that this particular diffuse echo event is transient in nature.

3. Discussion

The local magnetic field magnitude enhancement observed at 22:45:43 UT by MARSIS is unusually abrupt and large. Given its close proximity to the strong interplanetary shock observed at 22:44:36 UT by MAVEN, we believe that there is a causal relationship between the two. A pressure pulse caused by the sudden enhancement in the solar wind dynamic pressure is expected to propagate at the fast magnetosonic speed from the bow shock through the magnetosheath and the magnetic pileup region (MPR) down to the ionosphere, leading to compression of the entire Mars-solar wind interaction region and resulting magnetic field enhancement in the upper ionosphere [*Ma et al.*, 2014]. As noted in section 2.1, we expect the interplanetary shock passage at Mars Express at almost the same time as MAVEN if we neglect the propagation delay in the subsonic plasma below the bow shock. We also note that the interplanetary shock plane is estimated to sweep past the entire dayside bow shock within only 15 s ($[1.6\,R_M, 0, 0] \cdot \mathbf{N}/(\mathbf{V}_{SW} \cdot \mathbf{N}) \sim -14.3$ s, where 1.6 R_M is a typical subsolar distance of the bow shock, see Figure 3b). This suggests that most of the observed time lag of ~1 min must be attributed to the delayed propagation time of the pressure enhancement information from the bow shock to the Mars Express location.

To test this scenario, we make an order-of-magnitude estimate of the expected propagation time of the pressure pulse. We compute the fast magnetosonic speed in the magnetosheath, $V_{fms,sheath}$, by using magnetosheath parameters measured by MAVEN at 20:50 UT on 2 February 2017 (the MAVEN location at this time is denoted by the magenta plus sign in Figure 3e), an ion density of $n_i \sim 4$ cm^{-3}, an ion temperature of $T_i \sim 100$ eV, an electron temperature of $T_e \sim 40$ eV, and a magnetic field magnitude of $B \sim 10$ nT, resulting in $V_{fms,sheath} = \sqrt{(k_B T_e + 5/3 \times k_B T_i)/m_i + B^2/(\mu_0 m_i n_i)} \sim 178$ km/s, where k_B is Boltzmann's constant, m_i is the ion mass (assuming protons), and μ_0 is the vacuum permeability. We also obtain a measured magnetosheath flow of $V_{sheath} \sim 150$ km/s with a nearly zero radial component (diverging around Mars). We use MARSIS local measurements at ~500 km altitudes, an electron density of 400 cm^{-3} and a magnetic field of 25 nT, and assume that O^+ is the dominant ion species and that temperatures are negligibly small at these altitudes, to obtain the fast magnetosonic speed (which is approximately the Alfvén speed) in the MPR of $V_{fms,MPR} \sim 7$ km/s. We estimate the propagation time under the following simplifying assumptions: (i) the entire dayside bow shock is perturbed at the same time; (ii) in the magnetosheath, the pressure pulse propagates isotropically at $V_{fms,sheath}$ in the plasma frame which is moving at V_{sheath} circularly around Mars; (iii) in the MPR, the pressure pulse propagates isotropically at $V_{MPR,sheath}$ in a stagnant plasma (neglecting plasma flows); and (iv) the magnetosheath and MPR are bounded by the nominal boundary positions [*Trotignon et al.*, 2006] as illustrated in Figure 3e. We search for a quickest route connecting the bow shock and Mars Express with two straight lines in the magnetosheath and MPR. Figure 3e presents the obtained quickest route, which takes 99 s in total. The estimated total propagation time is roughly consistent with the observed response time of ~1 min within a factor of 2. Sources of errors include deviation from the simplified propagation speeds and difference between the nominal and instantaneous boundary positions. Though more sophisticated modeling is required to examine full details of the pressure pulse propagation in the Mars-solar wind system, we would conclude that the abrupt magnetic field enhancement measured by MARSIS in the upper ionosphere is likely to be caused by the sudden dynamic pressure enhancement associated with the interplanetary shock passage.

Here we briefly discuss why MARSIS did not detect similar magnetic field jumps more regularly. The uncommonness of similar events in the long-term MARSIS data may seem surprising, given the regular passage of interplanetary shocks at Mars. This can be explained by the combination of the following reasons:

1. The extremely sharp (<1 s) nature of the interplanetary shock passage on 2 February 2017 may cause the exceptionally abrupt enhancement in the ionospheric magnetic field. For other shocks with more gradual transitions, MARSIS will observe more slowly varying ionospheric magnetic fields, which may not satisfy our selection criteria.
2. Mars Express must be located near the periapsis at the time of the shock passage in order for MARSIS to measure the ionospheric response. As shown in Figure 1i, MARSIS operates in the ionospheric mode for limited portions of the time with many large data gaps.

The remote soundings of the topside ionosphere display several characteristic signatures which suggest deviation from a nominal, horizontally stratified ionosphere. First, the oblique echo is observed above the radial

crustal magnetic field (Figures 2e and 4b). Given the extremely stable presence of the oblique echoes and their close association with radial crustal fields [*Andrews et al.*, 2014] (see also Figures 2h–2k), we would not consider that the oblique echo observed at 22:43:27–22:45:43 UT is causally related to the interplanetary shock passage. We note that the oblique echo in Figure 2e does exhibit slightly different properties (echo intensity, thickness, and apex altitude) compared to those in Figures 2h–2k, possibly related to small differences in the orbital configuration. Second, we observe the diffuse echoes, which are indicative of irregularities in the ionosphere, shortly after the local magnetic field enhancement (Figure 2e). The considerably broadened echo (Figure 4c) suggests a severe deviation from the horizontally stratified ionosphere. Considering the transient nature of this diffuse echo event (no diffuse echoes are seen in Figures 2h–2k), we speculate that these irregular structures could be associated with perturbations in the topside ionosphere caused by the propagated pressure pulse originating from the interplanetary shock. Assuming that the pressure pulse propagates downward at a few kilometers per second from the Mars Express altitude (478 km) to the 1.7–1.8 MHz ionospheric echo altitude (~170–200 km), we can estimate the propagation time of ~1–3 min. This is roughly consistent with the time lag of 53 ± 7.54 s between the local magnetic field enhancement at 22:45:43 UT (Figure 2c) and the start time of the diffuse echo at 22:46:36 UT (Figure 2e). Thus, the timing analysis supports the pressure pulse perturbation scenario, but numerical simulations would be necessary to validate this hypothesis and identify the physical processes.

4. Conclusions

Based on the analysis of MAVEN and MARSIS data, we investigated the dynamic response of the topside ionosphere of Mars to an interplanetary shock passage. In response to the sudden dynamic pressure enhancement associated with the interplanetary shock, the ionospheric magnetic field magnitude increased abruptly with a time lag of ~1 min, which is consistent with the propagation time of a pressure pulse at the fast magnetosonic speed from the bow shock to the upper ionosphere. The remote soundings indicate the formation of highly irregular structures in the topside ionosphere, possibly caused by perturbations originating from the interplanetary shock passage.

Acknowledgments
The MARSIS investigation at the University of Iowa was supported by NASA through contract 1560641 with the Jet Propulsion Laboratory. MARSIS data are available through the Planetary Data System at http://pds-geosciences.wustl.edu. MAVEN data are publicly available through the Planetary Data System at https://pds-ppi.igpp.ucla.edu.

References

Akalin, F., D. Morgan, D. Gurnett, D. Kirchner, D. Brain, R. Modolo, M. Acuña, and J. Espley (2010), Dayside induced magnetic field in the ionosphere of Mars, *Icarus*, *206*(1), 104–111, doi:10.1016/j.icarus.2009.03.021.

Andrews, D. J., M. André, H. J. Opgenoorth, N. J. T. Edberg, C. Diéval, F. Duru, D. A. Gurnett, D. Morgan, and O. Witasse (2014), Oblique reflections in the Mars Express MARSIS data set: Stable density structures in the Martian ionosphere, *J. Geophys. Res. Space Physics*, *119*, 3944–3960, doi:10.1002/2013JA019697.

Berdichevsky, D. B., A. Szabo, R. P. Lepping, A. F. Viñas, and F. Mariani (2000), Interplanetary fast shocks and associated drivers observed through the 23rd solar minimum by Wind over its first 2.5 years, *J. Geophys. Res.*, *105*(A12), 27,289–27,314, doi:10.1029/1999JA000367.

Connerney, J., J. Espley, P. Lawton, S. Murphy, J. Odom, R. Oliversen, and D. Sheppard (2015), The MAVEN magnetic field investigation, *Space Sci. Rev.*, *195*, 257, doi:10.1007/s11214-015-0169-4.

Curry, S. M., et al. (2015), Response of Mars O+ pickup ions to the 8 March 2015 ICME: Inferences from MAVEN data-based models, *Geophys. Res. Lett.*, *42*, 9095–9102, doi:10.1002/2015GL065304.

Diéval, C., G. Stenberg, H. Nilsson, N. J. T. Edberg, and S. Barabash (2013), Reduced proton and alpha particle precipitations at Mars during solar wind pressure pulses: Mars express results, *J. Geophys. Res. Space Physics*, *118*, 3421–3429, doi:10.1002/jgra.50375.

Diéval, C., D. J. Andrews, D. D. Morgan, D. A. Brain, and D. A. Gurnett (2015), MARSIS remote sounding of localized density structures in the dayside Martian ionosphere: A study of controlling parameters, *J. Geophys. Res. Space Physics*, *120*, 8125–8145, doi:10.1002/2015JA021486.

Dubinin, E., M. Fraenz, J. Woch, F. Duru, D. Gurnett, R. Modolo, S. Barabash, and R. Lundin (2009), Ionospheric storms on Mars: Impact of the corotating interaction region, *Geophys. Res. Lett.*, *36*, L01105, doi:10.1029/2008GL036559.

Duru, F., D. A. Gurnett, T. F. Averkamp, D. L. Kirchner, R. L. Huff, A. M. Persoon, J. J. Plaut, and G. Picardi (2006), Magnetically controlled structures in the ionosphere of Mars, *J. Geophys. Res.*, *111*, A12204, doi:10.1029/2006JA011975.

Duru, F., D. A. Gurnett, D. D. Morgan, R. Modolo, A. F. Nagy, and D. Najib (2008), Electron densities in the upper ionosphere of Mars from the excitation of electron plasma oscillations, *J. Geophys. Res.*, *113*, A07302, doi:10.1029/2008JA013073.

Duru, F., D. A. Gurnett, D. D. Morgan, J. D. Winningham, R. A. Frahm, and A. F. Nagy (2011), Nightside ionosphere of Mars studied with local electron densities: A general overview and electron density depressions, *J. Geophys. Res.*, *116*, A10316, doi:10.1029/2011JA016835.

Edberg, N. J. T., et al. (2010), Pumping out the atmosphere of Mars through solar wind pressure pulses, *Geophys. Res. Lett.*, *37*, L03107, doi:10.1029/2009GL041814.

Ergun, R. E., M. W. Morooka, L. A. Andersson, C. M. Fowler, G. T. Delory, D. J. Andrews, A. I. Eriksson, T. McEnulty, and B. M. Jakosky (2015), Dayside electron temperature and density profiles at Mars: First results from the MAVEN Langmuir probe and waves instrument, *Geophys. Res. Lett.*, *42*, 8846–8853, doi:10.1002/2015GL065280.

Espley, J. R., W. M. Farrell, D. A. Brain, D. D. Morgan, B. Cantor, J. J. Plaut, M. H. Acuña, and G. Picardi (2007), Absorption of MARSIS radar signals: Solar energetic particles and the daytime ionosphere, *Geophys. Res. Lett.*, *34*, L09101, doi:10.1029/2006GL028829.

Futaana, Y., S. Barabash, A. Grigoriev, D. Winningham, R. Frahm, M. Yamauchi, and R. Lundin (2006), Global response of Martian plasma environment to an interplanetary structure: From ENA and plasma observations at Mars, *Space Sci. Rev.*, *126*(1-4), 315–332, doi:10.1007/s11214-006-9026-9.

Futaana, Y., et al. (2008), Mars Express and Venus Express multi-point observation's of geoeffective solar flare events in December 2006, *Planet. Space Sci.*, *56*(6), 873–880, doi:10.1016/j.pss.2007.10.014.
Gurnett, D., et al. (2008), An overview of radar soundings of the Martian ionosphere from the Mars Express spacecraft, *Adv. Space Res.*, *41*(9), 1335–1346, doi:10.1016/j.asr.2007.01.062.
Gurnett, D., D. Morgan, F. Duru, F. Akalin, J. Winningham, R. Frahm, E. Dubinin, and S. Barabash (2010), Large density fluctuations in the Martian ionosphere as observed by the Mars express radar sounder, *Icarus*, *206*(1), 83–94, doi:10.1016/j.icarus.2009.02.019.
Gurnett, D. A., et al. (2005), Radar soundings of the ionosphere of Mars, *Science*, *310*(5756), 1929–1933, doi:10.1126/science.1121868.
Halekas, J., E. Taylor, G. Dalton, G. Johnson, D. Curtis, J. McFadden, D. Mitchell, R. Lin, and B. Jakosky (2015), The solar wind ion analyzer for MAVEN, *Space Sci. Rev.*, *195*, 125–151, doi:10.1007/s11214-013-0029-z.
Hara, T., K. Seki, Y. Futaana, M. Yamauchi, M. Yagi, Y. Matsumoto, M. Tokumaru, A. Fedorov, and S. Barabash (2011), Heavy-ion flux enhancement in the vicinity of the Martian ionosphere during CIR passage: Mars express ASPERA-3 observations, *J. Geophys. Res.*, *116*, A02309, doi:10.1029/2010JA015778.
Huddleston, D. E., C. T. Russell, M. G. Kivelson, and J. G. Luhmann (1996), Time delays in the solar wind flow past Venus: Galileo-Pioneer Venus correlations, *J. Geophys. Res.*, *101*(E2), 4539–4546, doi:10.1029/95JE02774.
Jakosky, B. M., et al. (2015a), MAVEN observations of the response of Mars to an interplanetary coronal mass ejection, *Science*, *350*(6261), 210, doi:10.1126/science.aad0210.
Jakosky, B. M., et al. (2015b), The Mars Atmosphere and Volatile Evolution (MAVEN) mission, *Space Sci. Rev.*, *195*, 3–48, doi:10.1007/s11214-015-0139-x.
Jordan, R., et al. (2009), The Mars express MARSIS sounder instrument, *Planet. Space Sci.*, *57*(14-15), 1975–1986, doi:10.1016/j.pss.2009.09.016.
Larson, D. E., et al. (2015), The MAVEN solar energetic particle investigation, *Space Sci. Rev.*, *195*(1), 153–172, doi:10.1007/s11214-015-0218-z.
Ma, Y. J., X. Fang, A. F. Nagy, C. T. Russell, and G. Toth (2014), Martian ionospheric responses to dynamic pressure enhancements in the solar wind, *J. Geophys. Res. Space Physics*, *119*, 1272–1286, doi:10.1002/2013JA019402.
Mitchell, D. L., et al. (2016), The MAVEN solar wind electron analyzer, *Space Sci. Rev.*, *200*, 495–528, doi:10.1007/s11214-015-0232-1.
Modolo, R., G. M. Chanteur, and E. Dubinin (2012), Dynamic Martian magnetosphere: Transient twist induced by a rotation of the IMF, *Geophys. Res. Lett.*, *39*, L01106, doi:10.1029/2011GL049895.
Morgan, D. D., D. A. Gurnett, D. L. Kirchner, J. L. Fox, E. Nielsen, and J. J. Plaut (2008), Variation of the Martian ionospheric electron density from Mars Express radar soundings, *J. Geophys. Res.*, *113*, A09303, doi:10.1029/2008JA013313.
Morgan, D. D., et al. (2014), Effects of a strong ICME on the Martian ionosphere as detected by Mars Express and Mars Odyssey, *J. Geophys. Res. Space Physics*, *119*, 5891–5908, doi:10.1002/2013JA019522.
Morschhauser, A., V. Lesur, and M. Grott (2014), A spherical harmonic model of the lithospheric magnetic field of Mars, *J. Geophys. Res. Planets*, *119*, 1162–1188, doi:10.1002/2013JE004555.
Němec, F., D. D. Morgan, C. Diéval, D. A. Gurnett, and Y. Futaana (2014), Enhanced ionization of the Martian nightside ionosphere during solar energetic particle events, *Geophys. Res. Lett.*, *41*, 793–798, doi:10.1002/2013GL058895.
Nielsen, E., X.-D. Wang, D. A. Gurnett, D. L. Kirchner, R. Huff, R. Orosei, A. Safaeinili, J. J. Plaut, and G. Picardi (2007), Vertical sheets of dense plasma in the topside Martian ionosphere, *J. Geophys. Res.*, *112*, E02003, doi:10.1029/2006JE002723.
Opgenoorth, H. J., D. J. Andrews, M. Fränz, M. Lester, N. J. T. Edberg, D. Morgan, F. Duru, O. Witasse, and A. O. Williams (2013), Mars ionospheric response to solar wind variability, *J. Geophys. Res. Space Physics*, *118*, 6558–6587, doi:10.1002/jgra.50537.
Orosei, R., et al. (2015), Mars Advanced Radar for Subsurface and Ionospheric Sounding (MARSIS) after nine years of operation: A summary, *Planet. Space Sci.*, *112*, 98–114, doi:10.1016/j.pss.2014.07.010.
Sánchez-Cano, B., et al. (2017), Mars plasma system response to solar wind disturbances during solar minimum, *J. Geophys. Res. Space Physics*, *122*, 6611–6634, doi:10.1002/2016JA023587.
Schneider, N. M., et al. (2015), Discovery of diffuse aurora on Mars, *Science*, *350*(6261), aad0313, doi:10.1126/science.aad0313.
Slavin, J. A., et al. (2009), MESSENGER and Venus Express observations of the solar wind interaction with Venus, *Geophys. Res. Lett.*, *36*, L09106, doi:10.1029/2009GL037876.
Sonnerup, B. U. Ö., and L. J. Cahill (1967), Magnetopause structure and attitude from Explorer 12 observations, *J. Geophys. Res.*, *72*(1), 171–183, doi:10.1029/JZ072i001p00171.
Trotignon, J., C. Mazelle, C. Bertucci, and M. Acuña (2006), Martian shock and magnetic pile-up boundary positions and shapes determined from the Phobos 2 and Mars Global Surveyor data sets, *Planet. Space Sci.*, *54*(4), 357–369, doi:10.1016/j.pss.2006.01.003.
Ulusen, D., D. A. Brain, J. G. Luhmann, and D. L. Mitchell (2012), Investigation of Mars' ionospheric response to solar energetic particle events, *J. Geophys. Res.*, *117*, A12306, doi:10.1029/2012JA017671.
Venkateswara Rao, N., P. Mohanamanasa, and S. V. B. Rao (2017), Magnetically controlled density structures in the topside layer of the Martian ionosphere, *J. Geophys. Res. Space Physics*, *122*, 5619–5629, doi:10.1002/2016JA023545.